HHS Public Access

Author manuscript

Nat Struct Mol Biol. Author manuscript; available in PMC 2015 May 01.

Published in final edited form as:

Nat Struct Mol Biol. 2014 November ; 21(11): 981–989. doi:10.1038/nsmb.2903.

MacroH2A1.1 and PARP-1 cooperate to regulate transcription by promoting CBP-mediated H2B acetylation

Hongshan Chen[1], **Penelope D. Ruiz**[1], **Leonid Novikov**[1], **Alyssa D. Casill**[1], **Jong Woo Park**[1,2], and **Matthew J. Gamble**[1]

[1]Department of Molecular Pharmacology, Albert Einstein College of Medicine, Yeshiva University, Bronx, NY, USA

Abstract

The histone variant macroH2A1 regulates gene expression important for differentiation, stem cell reprogramming and tumor suppression. Here, we demonstrate that in primary human cells, macroH2A1 participates in two physically and functionally distinct types of chromatin either marked by H3K27me3 or nine histone acetylations. Using RNA-seq, we found that macroH2A1-regulated genes, which have roles in cancer progression, are specifically found in macroH2A1-containing acetylated chromatin. Of the two macroH2A1 variants, macroH2A1.1 and macroH2A1.2, the former is suppressed in cancer and can interact with PARP-generated poly(ADP-ribose). Through the recruitment of PARP-1, macroH2A1.1 promotes the CBP-mediated acetylation of H2B K12 and K120 which either positively or negatively regulates the expression of macroH2A1-target genes. While macroH2A1-regulated H2B acetylation is a common feature of primary cells, this regulation is typically lost in cancer cells. Consequently, our results provide important insight into macroH2A1.1's role in cancer suppression.

Introduction

The incorporation of histone variants into chromatin is a key mechanism used by eukaryotic cells to regulate transcription. The three macroH2A isoforms, macroH2A1.1, macroH2A1.2 and macroH2A2, contain an amino-terminal H2A-like region fused to a macrodomain by a flexible linker. Through their ability to regulate transcription, these histone variants have been implicated in a variety of processes including tumor suppression, inhibition of reprograming and differentiation[1-3].

Address correspondence to: Matthew J. Gamble, Department of Molecular Pharmacology, Albert Einstein College of Medicine, 1300 Morris Park Avenue, Golding 203, Bronx, NY 10461, USA. Phone: 718-430-2942; matthew.gamble@einstein.yu.edu.

[2]Present addresses: Department of Biochemistry and Molecular Biology, College of Pharmacy, Sungkyunkwan University, Korea (J.W.P.)

Author contributions:

H.C. designed and performed experiments, analyzed the data and wrote the manuscript. L.N., P.D.R. and J.W.P. performed experiments. A.D.C. performed the analysis of TCGA data. M.J.G. designed experiments, analyzed data and wrote the manuscript.

Accession Codes:

The GEO accession number for the ChIP-Seq and RNA-Seq data generated for this paper is GSE54847.

Macrodomains are roughly 25 kDa conserved globular domains which typically harbor the ability to interact with the NAD^+-derived, the post-translational modifications (PTMs) mono(ADP-ribose) and poly(ADP-ribose) (PAR)[4]. These PTMs are catalyzed by a family of ADP-ribosyltransferases, of which the most well studied member is PARP-1 (also known as ARTD1). PARP-1 has established roles in both DNA damage responses and transcriptional regulation[5]. Several macrodomain-containing proteins are recruited to sites of PARP-1 activity[6-8]. Additionally, the functions of macrodomain-containing proteins are often linked to their ability to interact with PARP-1-catalyzed PAR chains[6-10].

MacroH2A1.1 and macroH2A1.2 are splice variants of the same gene; each bearing a unique exon[11]. Like most macrodomains, macroH2A1.1's macrodomain can interact with NAD^+-derived ligands, such as PAR, while the macrodomains of macroH2A1.2 and macroH2A2 cannot[11]. This distinction is functionally important in cancer, where reduction in macroH2A1.1 occurs in several tumor types[10,12-14]. This alteration in macroH2A1.1 expression has important effects on both the proliferation and metastatic potential of cancer cells which appears to be due, in part, to the loss of macroH2A1's interaction with PARP-1 (refs. 10,15).

MacroH2A1 was originally localized to the inactive X chromosome (Xi) in female mammals and was therefore proposed to function as a repressor of transcription[16]. Together with DNA methylation, H3K27me3 and histone hypoacetylation, macroH2A1 participates in the multilayered mechanisms of transcriptional repression on the Xi[17]. However, macroH2A1 also occupies large domains spread across a substantial proportion of autosomal DNA[18]. An association between macroH2A1 and repressive H3K27me3 was found both on the Xi and in autosomal macroH2A1-enriched chromatin domains. Negative correlation between macroH2A1 and autosomal gene expression, further suggested a repressive role for macroH2A1 in transcription[18]. Several groups have shown that macroH2A1 represses transcription for a subset of genes and repetitive elements[18-26]. However, macroH2A1 is not exclusively a transcriptionally repressive factor; it has been shown to positively regulate a subset of the genes found in macroH2A1-containing domains[18,27]. MacroH2A1's ability to either positively or negatively regulate transcription highlights that there is still much to learn about this histone variant.

Here, we set out to determine how macroH2A1's interaction with its broader chromatin niche contributes to its ability to regulate transcription. We show that macroH2A1 does not exclusively localize to H3K27me3-containing facultative heterochromatin. A similar proportion of macroH2A1 associates with chromatin marked by a specific set of nine histone acetylations. Furthermore, we demonstrate that macroH2A1 positively regulates two of these acetylations, H2BK12ac and H2BK120ac, in primary cells. The ability of macroH2A1 to both regulate and associate with these acetylations is lost in cancer cells. Co-occupancy by macroH2A1 and the set of acetylations is a feature of genes regulated by macroH2A1. Specifically, the macroH2A1.1 variant and its ability to interact with PARP-1-catalyzed PAR chains are critical for the regulation of CBP-mediated H2B K12 and K120 acetylation and for the ability to regulate macroH2A1-target gene expression.

Results

MacroH2A1 occupies two distinct types of chromatin

The previously identified connection between macroH2A1 and H3K27me3 cannot, in itself, explain the more complicated association between macroH2A1 and transcriptional regulation[18]. To gain a more detailed understanding of histone PTMs associated with macroH2A1-containing chromatin, we performed chromatin immunoprecipitation coupled to sequencing (ChIP-seq) for macroH2A1 in IMR90 primary human lung fibroblasts (Supplementary Table 1). To analyze our ChIP-seq data, we developed an algorithm, called ISOR, which uses iterative segmentation to divide the genome into variable-length regions representing distinct binding states. Our macroH2A1 ChIP-seq data is highly reproducible and shows excellent correspondence with previous ChIP-chip data with the benefit of genome-wide coverage (Supplementary Fig. 1). Confirmation analysis across 54 genomic loci indicated a false discovery rate less than 0.02. MacroH2A1 occupies large regions of chromatin that can span hundreds of kilobases and occupies 33% of autosomal DNA (Supplementary Fig. 1).

By comparing our macroH2A1 ChIP-seq data to publically available ChIP-seq data for 26 histone marks in IMR90 cells[28], we found that macroH2A1 is enriched (odds ratio = 4) in chromatin marked by H3K27me3 (Fig. 1a,b and Supplementary Table 2). Surprisingly, macroH2A1-containing chromatin was also enriched (odds ratio between 2 and 4) for nine histone acetylations, including acetylation of H2B at K12, K15, K20, and K120, H3 at K4, K14, and K18, H4 at K91, and H2A at K5 (Fig. 1b and Supplementary Table 2). H3K27me3 marks repressed regions of the genome while this set of nine acetylations mark transcriptionally active regions (Supplementary Fig. 2). Furthermore, these macroH2A1-enriched histone PTMs segregate into two distinct types of chromatin; macroH2A1 either occupies regions marked by H3K27me3 or regions marked by the acetylations (Fig. 1c,d). By quantifying the degree of overlap between the ten macroH2A1-enriched PTMs across the genome, we demonstrated that the set of acetylations and H3K27me3 represent two distinct, largely non-overlapping chromatin environments (Fig. 1e,f).

Chromatin environment predicts gene regulation by macroH2A1

To understand how these different chromatin environments influence macroH2A1 function, we performed RNA-seq on control and macroH2A1-depleted IMR90 cells and identified 596 macroH2A1-regulated autosomal genes (Fig. 2a). IPA analysis indicated that macroH2A1 regulated genes are enriched for a variety of cancer related functions (Table 1 and Supplementary Table 3). Computational analysis of gene expression data from squamous cell lung cancer tumors indicated that macroH2A1-regulated genes, specifically those downregulated in macroH2A1-depleted IMR90 cells, are significantly enriched for genes with altered expression in lung cancer (Supplementary Fig. 2). Reduction of macroH2A1.1 levels, due to changes in alternative splicing are a hallmark of lung cancer[10,12]. We found that genes that positively correlated with changes in macroH2A1.1 splicing across the squamous cell lung cancer data are significantly enriched for genes positively regulated by macroH2A1 in IMR90 cells. Interestingly, loss of macroH2A1 in IMR90 cells enhanced cancer-relevant phenotypes including proliferation and anchorage-

independent growth (Supplementary Fig. 2). Overall, these findings support a role for macroH2A1 in suppression of oncogenesis and metastasis[10,12-15,29].

We used metagene analysis to identify distinguishing features of macroH2A1-regulated genes. When we examined the PTMs present at macroH2A1-regulated genes, we found a clear enrichment of the same acetylations enriched in macroH2A1-containing chromatin (Fig. 2b). We did not, however, observe enrichment of H3K27me3 at macroH2A1 regulated genes. We found that 35.6% of macroH2A1-regulated genes in IMR90 cells were downregulated upon macroH2A1 depletion, while 64.4% were upregulated (Fig. 2a). Marked differences in the levels of these acetylations were not observed in genes upregulated by macroH2A1 depletion compared to downregulated genes (Supplementary Fig. 3).

As an independent approach to determine the key features of genes regulated by macroH2A1, we categorized protein coding genes by their macroH2A1, H2BK12ac, and H3K27me3 occupancy, yielding eight categories (Supplementary Fig. 4). MacroH2A1-regulated genes were enriched in the two categories defined by macroH2A1 and H2BK12ac occupancy (Fig. 2c). Genes upregulated or downregulated upon macroH2A1 depletion showed a similar distribution across the eight categories (Supplementary Fig. 4). While genes co-occupied by macroH2A1, H2BK12ac and H3K27me3 were also enriched for macroH2A1-regulated genes, no other category marked by H3K27me3 was significantly enriched, suggesting H3K27me3 alone is not a predictor for genes regulated by macroH2A1, consistent with the conclusions from the meta-gene analysis. Together, these data suggest that, while they do not distinguish between genes positively or negatively regulated by macroH2A1, these acetylations are key determinants for regulation of macroH2A1-target genes.

MacroH2A1 regulates the acetylation of H2B K12 and K120

We hypothesized that macroH2A1 may influence local chromatin by regulating some macroH2A1-enriched PTMs. By monitoring each PTM associated with macroH2A1 in macroH2A1-depleted IMR90 cells, we demonstrated that macroH2A1 specifically promotes acetylation of H2B at K12 and K120 (Fig. 3a and Supplementary Fig. 5). We confirmed the role of macroH2A1 in promoting H2BK120ac and H2BK12ac in several additional primary cells including skin fibroblasts, hepatocytes, and prostate and mammary epithelium (Fig. 3b). Strikingly, macroH2A1-mediated regulation of H2BK12ac and H2BK120ac is unique to primary cells. When macroH2A1 was depleted from five cancer or transformed cell lines, no alteration in H2BK12ac or H2BK120ac was observed (Fig. 3b).

MacroH2A1 co-occupies 59% of regions marked by H2BK12ac or H2BK120ac, leaving 41% of these regions unoccupied by macroH2A1 (Fig. 1f). We hypothesized that macroH2A1 was directly and locally promoting H2BK12ac and H2BK120ac in macroH2A1-containing domains. Alternatively, macroH2A1 might globally affect these PTMs by regulating the expression of a histone acetyltransferase (HAT) or histone deacetylase (HDAC). To distinguish between these possibilities, we performed ChIP-qPCR for H2BK12ac and H2BK120ac in control and macroH2A1-depleted cells on 19 loci either containing or devoid of macroH2A1 (Fig. 3c). MacroH2A1 depletion reduced H2BK12ac

and H2BK120ac specifically inside macroH2A1-containing regions, indicating that macroH2A1 locally directs H2BK12ac and H2BK120ac. Additionally, these observations demonstrate that there are at least two pathways regulating H2B K12 and K120 acetylation operating in distinct regions, either dependent or independent on macroH2A1.

The ability of macroH2A1 to regulate H2B acetylation in primary but not cancer cells, suggests that cancer cells only use macroH2A1-independent mechanisms to maintain these acetylations. We hypothesized this was due to a lack of co-occupancy between macroH2A1 and the acetylations in cancer cells. To test this, mononucleosomes isolated from primary IMR90 cells and A549 lung cancer cells were immunoprecipitated with antibodies against H2BK12ac, H2BK120ac, H3K27me3 or H3K4me3 as a control. While macroH2A1 was enriched in H3K27me3-containing nucleosomes in IMR90 or A549 cells, macroH2A1 was only associated with H2B K12 and K120 acetylated nucleosomes in the IMR90 cells, and not in A549 (Fig. 3d). Therefore, the macroH2A1 chromatin environments in these two cell types are distinct, with macroH2A1 co-occupancy with H2B K12 and K120 acetylated chromatin absent in cancer cells.

MacroH2A1.1 specifically regulates H2BK12ac and H2BK120ac

We wondered why macroH2A1-mediated H2B acetylation does not occur in H3K27me3-containing regions of chromatin and why macroH2A1's regulation of these acetylations is a common feature of primary cells, but absent in cancer and transformed cells (Fig 3b). MacroH2A1 exists as either macroH2A1.1 or macroH2A1.2 splice variants. In primary cells, such as IMR90 lung fibroblasts, macroH2A1.1 accounts for approximately 50% of total macroH2A1 (ref. 10). By probing the mononucleosome immunoprecipitations described above with antibodies specific for each macroH2A1 variant, we found that macroH2A1.1 specifically localizes to H2B acetylated chromatin while macroH2A1.2 is most enriched in H3K27me3-conatining chromatin (Fig. 3d). Previous studies have demonstrated that macroH2A1 splicing is often altered in cancer, causing reduction of macroH2A1.1 (refs. 10,12,13). While the cancer cell lines assayed here have robust expression of total macroH2A1, there is a striking reduction in macroH2A1.1 levels compared to primary cells (Fig. 4a). Therefore, we hypothesized that macroH2A1.1 is specifically responsible for macroH2A1-mediated H2BK12ac and H2BK120ac.

To determine which macroH2A1 variant is responsible for regulating these acetylations, we ectopically expressed either variant in IMR90. Importantly, when we ectopically express macroH2A1 a poorly understood feedback mechanism represses expression of endogenous macroH2A1, leaving the ectopically expressed protein as the predominant isoform (Fig. 4b,c). When we ectopically expressed macroH2A1.1 we observed a modest increase in global H2BK12ac and H2BK120ac (Fig. 4c). When macroH2A1.2 was ectopically expressed, leading to depletion of macroH2A1.1, H2B K12 and K120 acetylation was reduced; highly reminiscent of the changes seen when total macroH2A1 was depleted. Using ChIP-qPCR, we monitored the effect of macroH2A1.1 overexpression in IMR90 cells on loci-specific acetylation of H2B K12 and K120. Overexpression of macroH2A1.1 led to increased macroH2A1 at macroH2A1-containing loci (Fig. 4d). Additionally, macroH2A1.1 overexpression also led to significantly increased macroH2A1 occupancy at many loci

normally devoid of macroH2A1. We found that H2B K12 and K120 acetylation increased at all loci where macroH2A1.1 overexpression led to increased macroH2A1 levels (Fig. 4d). Overall, these results define a specific role for macroH2A1.1 in promoting H2B K12 and K120 acetylation in primary cells.

Unlike macroH2A1.2, macroH2A1.1 interacts with NAD^+-derived ligands like PAR through its macrodomain[6,11]. We sought to determine if this distinction was critical for the ability of macroH2A1.1 to promote H2B K12 and K120 acetylation. To test this, we ectopically expressed point mutants (G224E and G314E) of macroH2A1.1 which cannot interact with NAD^+-derived ligands (Fig. 4b)[11]. Both macroH2A1.1 point mutants phenocopied ectopic expression of macroH2A1.2, where reduction of H2BK12ac and H2BK120ac was observed (Fig. 4c). However, the macrodomain of macroH2A1.1 alone cannot regulate H2BK12ac and H2BK120ac in trans. When fused to GFP, the macrodomain of macroH2A1.1 remains nuclear, but cannot be incorporated into chromatin[10]. When expressed in IMR90 cells, the GFP-macrodomain fusion is insufficient to alter H2B acetylation (Supplemental Fig. 6), indicating that both ligand binding and chromatin incorporation are required for macroH2A1.1 to regulate H2B acetylation.

The observation that regulation of H2B K12 and K120 acetylation is a specific function of macroH2A1.1 suggested that the loss of macroH2A1.1 expression typical in cancer may explain why these acetylations are not regulated by macroH2A1 in cancer cells. To test this we re-expressed macroH2A1.1 in A549 lung cancer cells. Re-expression of macroH2A1.1, or the mutants described in Figure 4b, did not alter global levels of H2B K12 and K120 acetylation (Supplementary Fig. 6). However, when we examined loci with increased macroH2A1 occupancy upon re-expression of macroH2A1.1, we found that macroH2A1.1 could enhance H2B K12 and K120 acetylation in the majority of these regions. In contrast, the acetylations were unaltered in regions devoid of ectopic macroH2A1.1. These data demonstrate macroH2A1.1's ability to interact with NAD^+-derived ligands is critical for regulation of H2B acetylation and explains the loss of macroH2A1-mediated regulation of these acetylations in cancer cells lacking macroH2A1.1.

PARP-1 is required for regulation of H2BK12ac and H2BK120ac

The data described above implicates macroH2A1.1's ligand binding function in regulating H2B K12 and K120 acetylation. Two of macroH2A1.1's ligands, PAR and monoADP-ribose, are covalent PTMs catalyzed by PARPs[30]. Through binding the ends of PAR chains, the macrodomain of macroH2A1.1 has been implicated in repression of PARP activity in vitro[20]. To determine if the activity of a PARP family member is required for macroH2A1-mediated regulation of H2BK12ac and H2BK120ac, we inhibited PARP enzymatic activity with PJ-34, a pan-specific PARP inhibitor[31]. Reminiscent of macroH2A1 depletion, PJ-34 treatment decreased H2B K12 and K120 acetylation in IMR90 primary lung fibroblasts, skin fibroblasts, prostate and mammary epithelium (Fig. 5a). PJ-34 does not affect H2B K12 and K120 acetylation in cancer cells. Other histone PTMs, like H3K4me3, were unaffected either in primary or cancer cells (Fig. 5a).

These data indicate PAR or mono-ADP-ribose is the critical ligand for macroH2A1.1-mediated regulation of H2B K12 and K120 acetylation in primary cells. Of the 18 members

of the PARP family, we focused on PARP-1 because it is the most abundant, widely expressed member[32]. Inhibition of PARP-1 with specific inhibitor BYK204165 (ref. 31) led to reductions in H2B K12 and K120 acetylation indicating that PARP-1 enzymatic activity plays a dominant role in this process (Fig. 5b). Finally, shRNA-mediated depletion of PARP-1 also reduced H2B K12 and K120 acetylation in primary cells but not cancer cells (Fig. 5c). Altogether, these data indicate that macroH2A1 and PARP-1 collaborate to regulate H2B K12 and K120 acetylation.

MacroH2A1 and PARP-1 collaborate to regulate gene expression

In addition regulating DNA repair, PARP-1 has been shown to regulate transcription through a variety of mechanisms[32]. We hypothesized that PARP-1 enzymatic activity is required for regulation of macroH2A1-target genes. We compared the effect of macroH2A1 depletion with PARP inhibition on 38 macroH2A1-regulated genes. Genes regulated by macroH2A1 were coordinately regulated by inhibition of PARP-1 activity either by PJ-34 or BYK204165 (Fig. 5d). In addition, ectopic expression of macroH2A1.2, which leads to macroH2A1.1 depletion (Fig 4c), mimics the effects seen in response to macroH2A1 depletion and PARP inhibition (Fig. 5d). Together, these results demonstrate that binding PARP-1-generated PAR is critical for regulation of macroH2A1 target genes.

Much of PARP-1's enzymatic activity is devoted to automodification. Previous studies have shown that macrodomain-containing proteins are recruited to sites of DNA-damage-induced PARP-1 activity[6-8]. We hypothesized that macroH2A1.1 regulates H2BK12ac and H2BK120ac and macroH2A1-target gene transcription by recruiting PAR-modified PARP-1. To test this model we performed ChIP-qPCR on a sample of eight genes either up- or downregulated upon macroH2A1 depletion (Supplementary Fig. 7). PARP-1 ChIP from macroH2A1-depleted cells demonstrated that PARP-1 association with macroH2A1-target genes was dependent on the presence of macroH2A1 (Fig. 5e and Supplementary Fig. 5). We confirmed the specificity of PARP-1 ChIP using PARP-1 depleted IMR90 cells (Supplementary Fig. 5). Next, we performed ChIP for PARP-1 in cells ectopically expressing macroH2A1.2, and depleted of macroH2A1.1 (Fig. 4c), demonstrating that PARP-1 association with macroH2A1-target genes was dependent on macroH2A1's ability to bind PAR (Fig. 5f and Supplementary Fig. 5). Finally, ChIP for PARP-1 in cells treated with PARP inhibitor, demonstrated that interaction of PARP-1 with macroH2A1-containing chromatin requires its enzymatic activity (Fig. 5g and supplementary Fig. 5). Overall, our data indicates that macroH2A1.1-mediated recruitment of PARP-1 is critical to regulate both H2B K12 and K120 acetylation and transcription of macroH2A1-target genes.

Histone acetylation regulates macroH2A1-target genes

To better understand the role of these acetylations in macroH2A1 regulated transcription, we treated macroH2A1-depleted cells with TSA, a class I and II HDAC inhibitor, or sirtinol, a class III HDAC inhibitor. Only TSA could restore global levels of H2B K12 and K120 acetylation back to that of controls, indicating that macroH2A1 opposes the activity of a class I or II HDAC (Fig. 6a). Using ChIP-qPCR analysis, we confirmed that TSA can reverse the loss of H2BK12ac and H2BK120ac in macroH2A1-depleted cells at macroH2A1-regulated genes (Fig. 6b). Functionally, TSA suppresses the effect of

macroH2A1 depletion on expression of macroH2A1 target genes (Fig. 6c). Acetylation is usually studied in relation to its positive role in transcriptional regulation, however, our data indicate that acetylation plays a critical role at genes either positively or negatively regulated by macroH2A1. These results indicate that macroH2A1-mediated regulation of H2B K12 and K120 acetylation is a critical feature of macroH2A1-mediated transcriptional regulation.

MacroH2A1.1 and PARP-1 recruit CBP to macroH2A1-target genes

We sought to identify the HAT responsible for catalyzing the macroH2A1 and PARP-1 mediated acetylation of H2B K12 and K120. While no interaction between macroH2A1 and a HAT has yet been reported, two reports from the literature led us to consider CBP as a possible candidate. 1) PARP-1 interacts with p300 and CBP[33,34]. 2) CBP regulates H2B acetylation during differentiation of trophoblast stem cells[35]. Using ChIP-qPCR, we determined that recruitment of CBP to macroH2A1 target genes requires macroH2A1 (Fig. 6d). We confirmed the CBP ChIP specificity using CBP-depleted IMR90 cells (Supplementary Fig. 5). Additionally, inhibition of PARP enzymatic activity prevents recruitment of CBP to these genes (Fig. 6e). Immunoblots from control and macroH2A1-depleted IMR90 cells demonstrate that lack of recruitment is not due to reduction of CBP levels (Supplementary Fig. 8). Two unrelated HATs, GCN5 and PCAF, failed to show altered binding in response to macroH2A1 depletion or PARP inhibition (Supplementary Fig. 5). Treatment of IMR90 cells with a CBP/p300 inhibitor C646[36], led to a decrease in H2BK12ac and H2BK120ac (Supplementary Fig. 8). In addition, IMR90 cells treated with C646 or CBP depleted (Supplementary Fig. 8) mirrored the changes in macroH2A1-target gene expression seen upon macroH2A1 depletion (Fig. 6f,g). Overall, these results demonstrate that recruitment of CBP is critical for macroH2A1 and PARP-1 to regulate H2BK12ac and H2BK120ac and regulate macroH2A1 target gene expression.

Discussion

Our data also indicates that macroH2A1 plays distinct roles in disparate chromatin environments. In the facultative heterochromatin of the Xi, DNA methylation, H3K27me3, histone deacetylases and macroH2A1 each contribute to redundant layers of transcriptional repression. Only combined treatment with DNA methyltransferase inhibitors, HDAC inhibitors and macroH2A1 shRNA reactivates silenced genes on the Xi[17]. The case is different for macroH2A1's role in its euchromatic environment described here, where macroH2A1 depletion alone is sufficient to alter the expression of many genes. The polarity of regulation is also distinct in each type of chromatin. In facultative heterochromatin macroH2A1 is implicated in transcriptional repression. Our data indicates that in macroH2A1-containing euchromatin, macroH2A1 plays either positive or negative roles. However, the determinants specifying macroH2A1's role as an activator or repressor are still unkown. Perhaps, distinguishing PTMs on macroH2A1 function as a switch, allowing it to play different roles in distinct environments. Interestingly, S137 phosphorylated macroH2A1 is excluded from heterochromatin[37], suggesting it might be such a distinguishing feature.

Trans-histone regulatory pathways, where alterations in one histone in a nucleosome affect a second histone modification, are central features of gene regulatory mechanisms. A classic example is the promotion of H3 K4 and K79 methylation in response to H2B K120 mono-ubiquitylation[38,39]. Histone variants have also been implicated in trans-histone regulatory dynamics. For example, H2A.Z nucleosomal incorporation is stimulated by H4K16ac[40]. Here we have shown that histone variants can play an upstream role in trans-histone regulatory pathways by showing macroH2A1 promotes H2BK12ac and H2BK120ac.

Our finding that macroH2A1.1 is specifically required for macroH2A1-mediated H2B K12 and K120 acetylation in primary cells leads to an apparent paradox about why H2BK12ac and H2BK120ac are high in cancer cells (Fig 4a). One might expect reduced levels of macroH2A1.1 to lead to reduced levels of those acetylations in cancer. However, we demonstrate that macroH2A1 does not regulate H2B K12 and K120 acetylation in cancer cells (Fig 3b). Furthermore, we show that macroH2A1 does not localize with sites of H2B K12 and K120 acetylation in cancer cells (Fig. 3d). Our data suggests that both macroH2A1-dependent and macroH2A1-independent mechanisms of H2B K12 and K120 acetylation exist in primary cells (Fig 3c). Therefore, upregulation of macroH2A1-independent pathways regulating acetylation of H2B K12 and K120 is common in cancer and may represent a mechanism by which cancer cells compensate for macroH2A1.1 loss. Further studies are required to determine how macroH2A1-independent H2B K12 and K120 acetylation is regulated and how this pathway is perturbed in cancer.

Our data demonstrates a requirement for PARP-1 in macroH2A1-regulated H2B K12 and K120 acetylation. PARP-1 can regulate transcription in a variety of ways, including several mechanisms where PARP-1 modulates chromatin structure[32]. PARP-1 acts as a transcriptional coactivator by promoting removal of linker histone H1 from nucleosomes[41]. PARP-1 maintains H3K4me3 levels by promoting the exclusion of KDM5B in a manner that requires PARP-1 enzymatic activity[42]. PARP-1 can also catalyze the addition of PAR chains onto histones[43,44]. Here we show that PARP-1 collaborates with macroH2A1 to promote H2B acetylation in a manner that requires both PARP-1 enzymatic activity and macroH2A1.1's ability to bind the ends of PAR chains. PARP-1 can also interact with p300 and CBP[33], which is implicated in the acetylation of H2B[35,45]. We have shown that through interaction with macroH2A1, PARP-1 recruits CBP to macroH2A1-target genes, identifying a new mechanism by which PARP-1 regulates chromatin function.

CBP and p300 are HATs that have been extensively studied as transcriptional coactivators recruited to chromatin by a variety of transcription factors[46]. The coactivator role of CBP is consistent with its requirement for the positive regulation of macroH2A1 target genes described here. Our data also indicates that CBP functions repressively at genes negatively regulated by macroH2A1. Repressive roles for CBP and p300 have been previously identified. For example, CBP and/or p300 are required the repression of Myb, YY1 and PLZF target genes[47-49]. Here we describe a novel repressive role for CBP at genes repressed by macroH2A1 that requires CBP enzymatic activity. While we don't yet understand the factors that specify positive or negative transcriptional regulation by macroH2A1, clearly CBP plays a role in both processes.

Recent studies have demonstrated tumor suppressive roles for macroH2A1 in several types of cancer[10,12-15]. Most of these studies specifically implicate macroH2A1.1 in tumor suppression[10,12,13,15]. Our results provide insight into the mechanism by which macroH2A1.1 suppresses cancer. We demonstrate that the ability of macroH2A1 and PARP-1 to mediate CBP-mediated acetylation of H2B K12 and K120 is lost in many cancer types (Fig. 7). Gene expression changes seen upon macroH2A1 depletion from primary cells mirrors the changes observed in cancers (Table 1 and Supplementary Table 3). The fact that the macroH2A1/PARP-1 pathway, through promotion of H2B K12 and K120 acetylation, regulates many genes whose expression is altered in cancer, combined with the observation that this pathway is disrupted in many cancer types, partially explains macroH2A1's role in cancer suppression.

Online Methods

Cell lines and Culture Conditions

IMR90 primary human fetal lung fibroblast cells (ATCC), hTERT-immortalized IMR90 (ref. 10), hTERT-immortalized BJ (ATCC) were cultured in MEM supplemented with 10% fetal bovine serum (FBS). A549 lung cancer cells (ATCC), HeLa cervical adenocarcinoma cells (ATCC) and MCF-7 human breast adenocarcinoma cells (ATCC) were cultured in RPMI supplemented with 10% FBS. Human embryonic kidney 293T cells (HEK293T, ATCC) and HepG2 hepatocyte carcinoma cells (ATCC) were cultured in DMEM supplemented with 10% FBS. Human hepatocyte cells (Lonza) were cultured in Clonetics™ Hepatocyte Maintenance Medium. Human prostate epithelial cells (Lonza) were cultured in Clonetics™ Prostate Epithelial Cell Growth Medium. Human mammary epithelial cells (Lonza) were cultured in Clonetics™ Mammary Epithelial Cell Growth Medium. Cell lines were routinely tested for mycoplasma contamination.

Cell lines depleted of macroH2A1, PARP-1 or Luciferase (as a control) were generated by retroviral-mediated expression of shRNA using the pSuper.Retro system (OligoEngine). The targeting sequence for macroH2A1 was 5′- GCGTGTGTTGTGGTGCTTTAT -3′[18]. The specificity of this sequence was confirmed with an independent shRNA, 5′-GCACTGATAGTTGGCATTA-3′[18]. The PARP-1 targeting sequence was 5′-GGGCAAGCACAGTGTCAAA-3′[41]. The Luciferase control shRNA targeting sequence was 5′-GATATGGGCTGAATACAAA-3′. The cells were selected and maintained under 0.5 mg/ml G418. Cell lines depleted of CBP or Luciferase were generated by lentiviral-mediated expression of shRNA using the pLKO.1 system (Open Biosystems). The targeting sequence for CBP was 5′-CCCGATAACTTTGTGATGTTT-3′, and the Luciferase control shRNA targeting sequence was 5′-CCTAAGGTTAAGTCGCCCTCG-3′. The cells were selected and maintained in 1 μg/ml puromycin. IMR90 or A549 cell lines expressing either green fluorescent protein (GFP), macroH2A1.1, macroH2A1.1 point mutants G224E, G314E, macroH2A1.2 or GFP-macro1.1 were generated by retroviral-mediated transduction using the pQCXIP expression system (Clontech) followed selection in 1 μg/ml puromycin. MacroH2A1 expression constructs harbor a carboxyl-terminal Flag tag.

Where indicated cells were treated with 10 μM PJ-34 (Enzo, ALX-270-289-M005), 10 μM BYK204165 (Sigma, B3188), 25 nM of Trichostain A (TSA) (Sigma, T8552), 75 μM of

Sirtinol (Sigma, s7942) and 20 μM C646 (p300 and CBP inhibitor, Millipore-Calbiochem, 382113).

Immunoblots and acid-extraction of histones

Cells were grown to 90% confluence in 10 cm dishes. The cells in one 10 cm dish were lysed in 100 μl of lysis buffer (10 mM Tris, pH 7.9, 0.1% Triton X-100, 100 mM NaCl, 1 mM EDTA, 5% glycerol, 1 mM DTT, 1× protease inhibitor cocktail). With incubation on ice for 30 min, the lysate was centrifuged at 14,000 rpm for 10 min at 4°C. The supernatant was collected as the detergent lysate. The pellet was resuspended in 80 μl 0.5 M HCl at 4°C for 2 hours under agitation to liberate acid-extractable proteins. The sample was spun at 14,000 rpm for 10 min at 4°C. The resulting supernatant was neutralized with 20 μl 2 M Tris. The resulting detergent lysates or acid extracts were subjected to SDS-PAGE and western blotting with antibodies listed (Supplementary Table 4). HRP-conjugated goat anti-mouse or anti-rabbit secondary antibody (Jackson Labs) was used for detection by ECL chemiluminescence following manufacturer's instructions (Thermo, Super Signal West Pico). All immunoblots have been repeated at least twice using independent biological samples.

Mononucleosome co-immunoprecipitation

The mononucleosome immunopreciptionation was performed essentially as described previously[50]. Four 15 cm dishes of IMR90 or A549 cells were grown to 90% confluence. The cells were collected, pelleted by centrifugation and resuspended in 1 ml of lysis buffer at 4°C for 30 min with agitation. The nuclei were collected by centrifugation at 4,500 rpm for 10 min. The nuclear pellet was then resuspended in 1 ml of MNase buffer (50 mM Trisl pH 7.4, 25 mM KCl, 12.5% glycerol, 10 mM CaCl2 and 4 mM MgCl2) with 22 U/μl micrococcal nuclease (MNase, NEB) and digested at 37°C for 15min. Then 116 μl MNase stop buffer (200 mM EDTA, 20 mM Tris 7.9 and 0.1 mg/ml RNAse) was added to stop the digestion. The reaction was then spun at 13,000 rpm for 10 min. 15 μl supernatant of the MNase reaction was kept as input and another 10 μl was used to confirming digestion to mononucleosomes. The DNA was cleared of protein with 0.4 mg/ml glycogen and proteinase K (2.5U/ml, Roche) in Txn stop buffer (20 mM EDTA, 0.2 M Nacl and 1% SDS) at 37°C for 30min. The DNA was extracted with phenol:chloroform:isoamyl alcohol (25:24:1) and ethanol precipitated. The resultant mono-nucleosome DNA was confirmed by running 1.5% agarose gel. Then immunoprecipitations were carried out using 150 μl supernatant of the MNase reaction, 200 μl HEGTw/300 buffer (20mM Tris PH 7.9, 1mM EDTA, 5% Glycerol, 0.1% Tween-20, 300mM NaCl), 40 μl Protein A beads and either no antibody (negative control), or antibody against H2BK12ac (10 μl), H2BK120ac (10 μl), H3K4me3 (2 μl) or H3K27me3 (3 μl). The reactions were rocked at 4°C for 2 hours. The beads were spun at 4,000 rpm for 3 min and washed three times in HEGTw/300 buffer. The resulting beads were treated with elution buffer (100 mM sodium bicarbonate, 1% SDS) at room temperature for 20 min. The eluted mono-nucleosome complexes were run on 10% or 20% SDS polyacrylamide gels for macroH2A1, macroH2A1.1, macroH2A1.2 and H3 detection.

Chromatin Immunoprecipitation (ChIP)

ChIP was performed essentially as described previously[18]. Briefly, cells were grown to 90% confluence in 15 cm dishes, cross-linked with 1% formaldehyde in PBS at room temperature for 10 min, then quenched in 125 mM glycine for 5 min. The cells were washed with cold PBS once and were collected by centrifugation and sonicated in lysis buffer (50mM Tris pH 7.9, 10 mM EDTA, 1% SDS, protease inhibitor cocktail and 1 mM DTT) to generate chromatin fragments ~500 bp in length. The material was clarified by 10 min centrifugation at 14,000 rpm and 4 °C, and 20 μl supernatant was used as input for quantitation. The remaining supernatant was diluted 10-fold in dilution buffer (20 mM Tris pH 7.9, 2 mM EDTA, 150 mM NaCl, 0.5% Triton X-100, protease inhibitor cocktail and 1 mM DTT), and pre-cleared with 20 μl protein A-agarose beads at 4°C for 3 hours. The supernatant was used in immunoprecipitations at 4°C overnight with antibodies against histone H3 (4 μl), macroH2A1 (8 μl), H2BK12ac (5 μl), H2BK120ac (5 μl), PARP-1 (20 μl), CBP (5 μl), GCN5 (10 μl), PCAF(10 μl) as indicated, then incubated with 40 μl protein A-agarose beads at 4°C for 2 hr. No-antibody (NA) controls were always included. The immunoprecipitated DNA was cleared of protein by digestion with 0.4 mg/ml glycogen and proteinase K (0.45 mg/ml, Roche) in Txn stop buffer at 37°C for 1 hour. The DNA was then extracted with phenol:chloroform:isoamyl alcohol (25:24:1) and ethanol precipitated. Quantitative real-time PCR (qPCR) using SYBR Green (Invitrogen) was used to determine enrichment of immunoprecipitated material relative to input using gene-specific primers to the specified regions (Supplementary Table 5).

ChIP-Seq Experiments and Analyses

MacroH2A1 ChIP from two biological replicates, performed as described above was used for library construction. DNA fragments were repaired using T4 DNA Polymerase (NEB) and T4 DNA Polynucleotide kinase (NEB) in T4 DNA ligase buffer (NEB). Next, dA ends were generated by employing Klenow Fragment (3′->5′ exo-, NEB), in Buffer 2 (NEB). Adapter ligation reactions were performed using indexed adapters and Quick Ligase (NEB). Ligation-mediated PCR was performed using Phusion High-Fidelity DNA Polymerase (NEB). The libraries were visualized on 2% E-Gel® Agarose Gels (Invitrogen). Sequencing for macroH2A1 ChIPs were performed on an Illumina HiSeq2500. Sequences reads were mapped to human genome version hg19 using ELAND version 1.7.0 (Illumina). Mapped reads were uploaded to GEO (GSE54847). Sequencing reads for 26 additional histone marks in IMR90 cells were downloaded from the GEO website (GSE16256).

Due to the tendency of many chromatin marks, including macroH2A1, to be distributed in broad domains and not sharp peaks, many peak-finding algorithms that perform well for ChIP-seq data of transcription factors fail for chromatin components and modifications. To overcome this drawback, we developed a novel algorithm called ISOR (Iterative Segmentation of Ordered Reads), to identify significantly enriched and depleted regions in ChIP-seq data. The details of the ISOR algorithm will be described elsewhere. Briefly, the ISOR algorithm works on the individual sequence reads directly without any preprocessing required. As its name suggests, beginning with the whole genome, ISOR applies an iterative segmentation algorithm, creating smaller and smaller genomic segments that best describe the local statistically significant fluctuations in the data. There are two required and one

optional parameter that can be specified, fragment length, critical segmentation p value and the optional sequencing gap length. The fragment length is used to shift the read to the theoretical center of a sequenced fragment (300 bp in this study). The critical segmentation p value (0.01 in this study) triggers the splitting of a parent segment into two smaller segments. At the end of the analysis the sequencing reads have been segmented into a set of contiguous non-overlapping windows or segments, each of which represents a distinct state of enrichment from its neighboring segments. It is often useful to remove gaps (1000 bp in this study) that do not contain sequencing reads in either the input or ChIP data sets.

ISOR functions in a three step loop. 1) A segment consisting of N ordered reads (where A = number of reads from the ChIP sequencing and B = number of reads from the input sequencing) is scanned for the point in the segment where the proportion of reads from the ChIP maximally deviates from what would be expected from a hypergeometric distribution of A ChIP reads and B input reads. 2) An extreme value distribution is then used to model the expected distribution of maximal deviations under the null hypothesis that ChIP and input reads are distributed hypergeometrically. The extreme value distribution has two parameters, location (μ) and scale (β).

$$\mu = 0.75g$$
$$\beta = 0.2g$$
$$where \quad g = \frac{A}{\sqrt{\frac{A*B}{N}}}$$

The extreme value distribution is then used to determine the probability of finding a maximal deviation equal to or more extreme than that found in the actual data. 3) If the probability of obtaining the observed deviation is less than the critical segmentation p value, the parent segment is split at that point into two child segments. The process continues iteratively until none of the segments have a maximal deviation that passes the critical p value.

Once complete, the genome will have been segmented into a collection of contiguous variable-length, non-overlaping windows, each of which represents a homogenous binding state. The ChIP signal (enrichment) can then be represented by the $\log_2$ odds ratio of ChIP and input reads.

$$log_2\,(odds \quad ratio) = log_2\left(\frac{A_{in}/B_{in}}{A_{out}/B_{out}}\right)$$

Where, A_{in} and B_{in} represent the number of ChIP and input reads inside the segment, respectively, and A_{out} and B_{out} represent the number of ChIP and input reads mapped to the rest of the genome, respectively. The significance of the enrichment or depletion is then estimated using a binomial distribution where A_{in} represents the number of successes, the number of trials is $A_{in} + B_{in}$ and the probability of success is $A_{total}/(A_{total} + B_{total})$.

ISOR outputs the analysis as a gappedPeak file (http://genome.ucsc.edu/FAQ/FAQformat.html), were the signalValue is given as the $\log_2$ odds ratio. ISOR also produces a bedGraph file for visualization purposes where the score is given as the $\log_2$ odds ratio. Visualization of the bedGraph files was performed with the GenPlay program (http://genplay.einstein.yu.edu/wiki/index.php/Web_Start)[51]. All area-proportional Venn diagrams were created with eulerAPE (http://www.eulerdiagrams.org/eulerAPE).

For metagene analysis, the coordinates for a set of 50 relatively positioned bins around all protein coding genes in ens67 (Ensemble) was generated. The 50 gene relative bins included 10 one kb bins upstream of the most 5′ TSS, 30 bins of roughly equal size (*gene length/*30) between the TSS and end of the gene, and 10 one kb bins downstream of the gene end. If the gene length was not evenly divisible by 30, the remainder was included in the 15th intragenic bin. Log_2 odds ratio values were assigned to each bin by alignment of the bin to the ISOR generated segmentation data. If a bin spanned more than one segment, then the degree of overlap between the segments and the bin was used to calculate a weighted average. The genes were then separated into groups based on the RNA-seq gene expression data (this study) or previously published GRO-seq data (GSE13518)[52].

The ChIP-seq data in the main text is from macroH2A1 ChIP replicate 1. Importantly, all results obtained from replicate 1 were reproducible in replicate 2. Given the enrichment of macroH2A1 on the Xi and the fact that IMR90 cells contain both an active and inactive X chromosome which are indistinguishable by sequencing, all ChIP-seq analysis has been subset for autosomal chromatin.

RNA Purification and RT-qPCR

mRNA levels were analyzed by reverse transcription followed by quantitative PCR (RT-qPCR). RNA was isolated using TriPure (Roche) according to the manufacturer's protocol. The RNA was reverse transcribed using Moloney murine leukemia virus (MMLV) reverse transcriptase (Invitrogen) and an dT_{18} primer. cDNA, SYBR Green PCR master mix, and forward and reverse primers were used in 45 cycles of amplification (95°C for 15 sec, 60°C for 1 min) following 10 min incubation at 95°C using LightCycler 480 (Roche). The efficiency-corrected threshold cycle (ΔCT) method was used to determine the relative levels of RNA[53]. For transcription analysis, the expression was normalized to ACTB. Melting curve analysis was performed to ensure specificity. Primer sequences are listed in Supplementary Table 6.

RNA-Seq and analyses

RNA-seq was performed on three biological replicates of IMR90 cells with shRNA targeting macroH2A1 or Luciferase grown to 90% confluence in 6-wells dishes. Total RNA was extracted using Tripure Isolation Reagent (Roche). RNA samples were treated with RNase-free DNaseI and purified using the RNeasy Mini Kit (QIAGEN). The RNA was depleted of ribosomal RNA using Ribo-Zero rRNA Removal Kit (Human/Mouse/Rat) (Epicentre). cDNA was then generated using SuperScript® III First-Strand Synthesis System (Invitrogen) according to the manufacturer's instructions. The second strand was generated using E. coli DNA ligase (Invitrogen), E. coli DNA polymerase (Invitrogen), and

dUTP, dCTP, dATP, and dGTP set (10 μmol each, Promega), in the Second Strand Buffer (Invitrogen). Then the cDNA were sheared with Covaris to roughly 300 bp and purified with MinElute columns (Qiagen). The 3′ and 5′ ends were repaired using T4 DNA Polymerase (NEB) and T4 DNA Polynucleotide kinase (NEB) in T4 DNA ligase buffer (NEB). dA ends were generated using Klenow Fragment (3′->5′ exo-, NEB), in Buffer 2 (NEB). Adapter ligation was performed using indexed adapters and Quick Ligase (NEB). The products were used as the template for UNG (Fermentas) treatment and PCR amplification using Phusion High-Fidelity DNA Polymerase (NEB). The libraries were visualized on 2% E-Gel® Agarose Gels (Invitrogen). The barcoded libraries were sequenced on a single lane of a HiSeq2500 (Illumina).

Sequencing reads were trimmed of barcodes and aligned to the human genome (hg19) using GSNAP version 2012-07-12[54]. The reads were then binned into genes (Ensemble ens67) using HTSeq version v0.5.3p3 (http://www-huber.embl.de/users/anders/HTSeq/doc/index.html). Identification of differential gene expression between the Luciferase and macroH2A1 conditions using an adjusted p value cutoff of 0.05 and a $\log_2$ fold change cutoff of 0.6 was performed with DESeq (version 1.10.1)[55]. The RNA-seq data have been uploaded to the GEO website (GSE54847). Enriched functional annotations among genes regulated by depletion of macroH2A1 were determined with Ingenuity Pathway Analysis (Ingenuity Systems, version 18030641). The associated p values were adjusted for multiple testing using the Benjamini-Hochberg method.

TCGA dataset gene expression analysis

The results published here are in part based upon data generated by TCGA Research Network: http://cancergenome.nih.gov/. Identification of differential gene expression between primary tumor and solid tissue normal samples in the TCGA lung squamous cell carcinoma (LUSC) dataset (http://unc.edu_LUSC.IlluminaHiSeq_RNASeqV2.Level_3.1.8.0/) was performed using DESeq (version1.10.1), with the cutoffs described above. This group of genes (regulated in the LUSC dataset) was compared to genes regulated by macroH2A1, as were genes upregulated in both groups and downregulated in both groups, using three Fisher's exact tests to determine the significance of the overlap between groups. We determined the fractional splicing of macroH2A1.1 specifically for each sample in the LUSC dataset by identifying the sequencing reads associated with the macroH2A1.1 and macroH2A1.2 specific splice junctions and calculating the percent of reads from macroH2A1.1 transcripts. A Pearson correlation coefficient was calculated for each gene, correlating the read counts for that gene to the macroH2A1.1 percent splicing in each sample, using a p value cutoff of 1×10^{-10} and a correlation coefficient cutoff of 0.3. The significance of overlap between genes correlated to changes in macroH2A1.1 expression and genes regulated by macroH2A1 was determined using a Fisher's exact test. Two additional Fisher's exact tests determined the significance of overlap between genes positively correlated with macroH2A1.1 expression and genes downregulated by macroH2A1, and between genes negatively correlated with macroH2A1.1 expression and genes upregulated by macroH2A1.

Cell proliferation assays

To detect the effect of macroH2A1 on cell growth potential, IMR90 cells with shRNA against Luc or macroH2A1 were plated in 6-well dishes at 5×10^4 cells/well. One well was counted with a hemocytometer (Hausser Scientific) on the days indicated. To access the role of macroH2A1 loss on anchorage-independent growth, soft-agar colony formation assays were performed essentially as described[56]. 5,000 cells/plate were plated in 0.35% noble agar on top of a 0.5% noble agar layer in 35 mm dishes, in triplicate. After six weeks, colonies were stained with 0.005% crystal violet solution, photographed and counted in four different fields using a dissecting microscope.

Statistical analysis

All loci specific ChIP and RT-qPCR experiments have been repeated 3 times. Results obtained are presented as means ± SEM. Two-tailed Student's t-tests were used to determine the significance of differences between samples indicated in figures. Fisher exact tests have been to determine the significance of enrichment in count data.

Supplementary Material

Refer to Web version on PubMed Central for supplementary material.

Acknowledgements

We thank S. B. Horwitz, C. S. Rubin, J. M. Backer and C. W. Chow from Albert Einstein College of Medicine for sharing equipment and reagents. We thank T. Zhang (Regeneron Pharmaceuticals) for critical reading of the manuscript. The high-throughput sequencing was performed by the Einstein Epigenomics Core Facility. We thank specimen donors and University of North Carolina TCGA genome characterization center for their contributions to the LUSC data set from The Cancer Genome Atlas. This work was supported by the US National Institutes of Health training grant 5T32GM007491-38 (P.D.R.) and grant R01CA155232 (M.J.G.).

References

1. Cantariño N, Douet J, Buschbeck M. MacroH2A - An epigenetic regulator of cancer. Cancer Lett. 2013; 336:247–52. [PubMed: 23531411]
2. Creppe C, Posavec M, Douet J, Buschbeck M. MacroH2A in stem cells: a story beyond gene repression. Epigenomics. 2012; 4:221–227. [PubMed: 22449192]
3. Gamble M, Kraus WL. Multiple facets of the unique histone variant macroH2A: From genomics to cell biology. Cell Cycle. 2010; 9:70–69.
4. Karras GI, et al. The macro domain is an ADP-ribose binding module. EMBO J. 2005; 24:1911–20. [PubMed: 15902274]
5. Gibson, B. a; Kraus, WL. New insights into the molecular and cellular functions of poly(ADP-ribose) and PARPs. Nat. Rev. Mol. Cell Biol. 2012; 13:411–24. [PubMed: 22713970]
6. Timinszky G, et al. A macrodomain-containing histone rearranges chromatin upon sensing PARP1 activation. Nat. Struct. Mol. Biol. 2009; 16:923–9. [PubMed: 19680243]
7. Gottschalk AJ, et al. Poly(ADP-ribosyl)ation directs recruitment and activation of an ATP-dependent chromatin remodeler. Proc. Natl. Acad. Sci. U. S. A. 2009; 106:13770–4. [PubMed: 19666485]
8. Ahel D, et al. Poly(ADP-ribose)-dependent regulation of DNA repair by the chromatin remodeling enzyme ALC1. Science. 2009; 325:1240–3. [PubMed: 19661379]
9. Gottschalk AJ, Trivedi RD, Conaway JW, Conaway RC. Activation of the SNF2 family ATPase ALC1 by poly(ADP-ribose) in a stable ALC1·PARP1·nucleosome intermediate. J. Biol. Chem. 2012; 287:43527–32. [PubMed: 23132853]

10. Novikov L, et al. QKI-mediated alternative splicing of the histone variant MacroH2A1 regulates cancer cell proliferation. Mol. Cell. Biol. 2011; 31:4244–55. [PubMed: 21844227]
11. Kustatscher G, Hothorn M, Pugieux C, Scheffzek K, Ladurner AG. Splicing regulates NAD metabolite binding to histone macroH2A. Nat. Struct. Mol. Biol. 2005; 12:624–5. [PubMed: 15965484]
12. Sporn JC, et al. Histone macroH2A isoforms predict the risk of lung cancer recurrence. Oncogene. 2009; 28:3423–8. [PubMed: 19648962]
13. Sporn JC, Jung B. Differential regulation and predictive potential of MacroH2A1 isoforms in colon cancer. Am. J. Pathol. 2012; 180:2516–26. [PubMed: 22542848]
14. Kapoor A, et al. The histone variant macroH2A suppresses melanoma progression through regulation of CDK8. Nature. 2010; 468:1105–9. [PubMed: 21179167]
15. Dardenne E, et al. Splicing switch of an epigenetic regulator by RNA helicases promotes tumor-cell invasiveness. Nat. Struct. Mol. Biol. 2012 doi:10.1038/nsmb.2390.
16. Costanzi C, Pehrson JR. Histone macroH2A1 is concentrated in the inactive X chromosome of female mammals. Nature. 1998; 393:599–601. [PubMed: 9634239]
17. Hernández-Muñoz I, et al. Stable X chromosome inactivation involves the PRC1 Polycomb complex and requires histone MACROH2A1 and the CULLIN3/SPOP ubiquitin E3 ligase. Proc. Natl. Acad. Sci. U. S. A. 2005; 102:7635–40. [PubMed: 15897469]
18. Gamble MJ, Frizzell KM, Yang C, Krishnakumar R, Kraus WL. The histone variant macroH2A1 marks repressed autosomal chromatin, but protects a subset of its target genes from silencing. Genes Dev. 2010; 24:21–32. [PubMed: 20008927]
19. Changolkar LN, Pehrson JR. macroH2A1 histone variants are depleted on active genes but concentrated on the inactive X chromosome. Mol. Cell. Biol. 2006; 26:4410–20. [PubMed: 16738309]
20. Ouararhni K, et al. The histone variant mH2A1.1 interferes with transcription by down-regulating PARP-1 enzymatic activity. Genes Dev. 2006; 20:3324–36. [PubMed: 17158748]
21. Doyen C, An W. Mechanism of polymerase II transcription repression by the histone variant macroH2A. Mol. Cell. Biol. Cell. Biol. 2006; 26:1156–1164.
22. Changolkar LN, et al. Developmental changes in histone macroH2A1-mediated gene regulation. Mol. Cell. Biol. 2007; 27:2758–64. [PubMed: 17242180]
23. Changolkar LN, Singh G, Pehrson JR. macroH2A1-dependent silencing of endogenous murine leukemia viruses. Mol. Cell. Biol. 2008; 28:2059–65. [PubMed: 18195046]
24. Buschbeck M, et al. The histone variant macroH2A is an epigenetic regulator of key developmental genes. Nat. Struct. Mol. Biol. 2009; 16:1074–9. [PubMed: 19734898]
25. Cong R, et al. macroH2A1 histone variant represses rDNA transcription. Nucleic Acids Res. 2014; 42:181–92. [PubMed: 24071584]
26. Kim J-M, Heo K, Choi J, Kim K, An W. The histone variant MacroH2A regulates Ca(2+) influx through TRPC3 and TRPC6 channels. Oncogenesis. 2013; 2:e77. [PubMed: 24165580]
27. Choo JH, Kim J, Do, Kim J. MacroH2A1 knockdown effects on the Peg3 imprinted domain. BMC Genomics. 2007; 8:479. [PubMed: 18166131]
28. Bernstein BE, et al. The NIH Roadmap Epigenomics Mapping Consortium. Nat. Biotechnol. 2010; 28:1045–8. [PubMed: 20944595]
29. Rappa F, et al. Immunopositivity for histone macroH2A1 isoforms marks steatosis-associated hepatocellular carcinoma. PLoS One. 2013; 8:e54458. [PubMed: 23372727]
30. Hottiger MO, Hassa PO, Lüscher B, Schüler H, Koch-Nolte F. Toward a unified nomenclature for mammalian ADP-ribosyltransferases. Trends Biochem. Sci. 2010; 35:208–19. [PubMed: 20106667]
31. Eltze T, et al. Imidazoquinolinone, Imidazopyridine, and Isoquinolindione Derivatives as Novel and Potent Inhibitors of the Poly (ADP-ribose) Polymerase (PARP): A Comparison with Standard PARP Inhibitors. 2008; 74:1587–1598.
32. Kraus WL, Hottiger MO. PARP-1 and gene regulation: progress and puzzles. Mol. Aspects Med. 2013; 34:1109–23. [PubMed: 23357755]

33. Hassa PO, et al. Acetylation of poly(ADP-ribose) polymerase-1 by p300/CREB-binding protein regulates coactivation of NF-kappaB-dependent transcription. J. Biol. Chem. 2005; 280:40450–64. [PubMed: 16204234]
34. Hassa PO, Buerki C, Lombardi C, Imhof R, Hottiger MO. Transcriptional coactivation of nuclear factor-kappaB-dependent gene expression by p300 is regulated by poly(ADP)-ribose polymerase-1. J. Biol. Chem. 2003; 278:45145–53. [PubMed: 12960163]
35. Abell AN, et al. MAP3K4/CBP-regulated H2B acetylation controls epithelial-mesenchymal transition in trophoblast stem cells. Cell Stem Cell. 2011; 8:525–37. [PubMed: 21549327]
36. Bowers EM, et al. Virtual ligand screening of the p300/CBP histone acetyltransferase: identification of a selective small molecule inhibitor. Chem. Biol. 2010; 17:471–82. [PubMed: 20534345]
37. Bernstein E, et al. A phosphorylated subpopulation of the histone variant macroH2A1 is excluded from the inactive X chromosome and enriched during mitosis. Proc. Natl. Acad. Sci. U. S. A. 2008; 105:1533–8. [PubMed: 18227505]
38. Briggs SD, et al. Gene silencing: trans-histone regulatory pathway in chromatin. Nature. 2002; 418:498. [PubMed: 12152067]
39. Sun Z-W, Allis CD. Ubiquitination of histone H2B regulates H3 methylation and gene silencing in yeast. Nature. 2002; 418:104–8. [PubMed: 12077605]
40. Shia W-J, Li B, Workman JL. SAS-mediated acetylation of histone H4 Lys 16 is required for H2A.Z incorporation at subtelomeric regions in Saccharomyces cerevisiae. Genes Dev. 2006; 20:2507–12. [PubMed: 16980580]
41. Krishnakumar R, et al. Reciprocal binding of PARP-1 and histone H1 at promoters specifies transcriptional outcomes. Science. 2008; 319:819–21. [PubMed: 18258916]
42. Krishnakumar R, Kraus WL. PARP-1 regulates chromatin structure and transcription through a KDM5B-dependent pathway. Mol. Cell. 2010; 39:736–49. [PubMed: 20832725]
43. Messner S, et al. PARP1 ADP-ribosylates lysine residues of the core histone tails. Nucleic Acids Res. 2010; 38:6350–62. [PubMed: 20525793]
44. Martinez-Zamudio R, Ha HC. Histone ADP-ribosylation facilitates gene transcription by directly remodeling nucleosomes. Mol. Cell. Biol. 2012; 32:2490–502. [PubMed: 22547677]
45. Schiltz RL. Overlapping but Distinct Patterns of Histone Acetylation by the Human Coactivators p300 and PCAF within Nucleosomal Substrates. J. Biol. Chem. 1999; 274:1189–1192. [PubMed: 9880483]
46. Bedford DC, Kasper LH, Fukuyama T, Brindle PK. Target gene context influences the transcriptional requirement for the KAT3 family of CBP and p300 histone acetyltransferases. Epigenetics. 2010; 5:9–15. [PubMed: 20110770]
47. Guidez F, et al. Histone acetyltransferase activity of p300 is required for transcriptional repression by the promyelocytic leukemia zinc finger protein. Mol. Cell. Biol. 2005; 25:5552–5566. [PubMed: 15964811]
48. Sankar N, et al. p300 provides a corepressor function by cooperating with YY1 and HDAC3 to repress c-Myc. Oncogene. 2008; 27:5717–28. [PubMed: 18542060]
49. Zhao L, et al. Integrated genome-wide chromatin occupancy and expression analyses identify key myeloid pro-differentiation transcription factors repressed by Myb. Nucleic Acids Res. 2011; 39:4664–79. [PubMed: 21317192]

Online References

50. Kim MY, Mauro S, Gévry N, Lis JT, Kraus WL. NAD+-dependent modulation of chromatin structure and transcription by nucleosome binding properties of PARP-1. Cell. 2004; 119:803–14. [PubMed: 15607977]
51. Lajugie J, Bouhassira EE. GenPlay, a multipurpose genome analyzer and browser. Bioinformatics. 2011; 27:1889–93. [PubMed: 21596789]
52. Core L, Waterfall J, Lis J. Nascent RNA sequencing reveals widespread pausing and divergent initiation at human promoters. Science (80-.). 2008; 322:1845–1848.

53. Schefe JH, Lehmann KE, Buschmann IR, Unger T, Funke-Kaiser H. Quantitative real-time RT-PCR data analysis: current concepts and the novel “gene expression’s CT difference” formula. J. Mol. Med. (Berl). 2006; 84:901–10. [PubMed: 16972087]

54. Wu TD, Nacu S. Fast and SNP-tolerant detection of complex variants and splicing in short reads. Bioinformatics. 2010; 26:873–81. [PubMed: 20147302]

55. Anders S, Huber W. Differential expression analysis for sequence count data. Genome Biol. 2010; 11:R106. [PubMed: 20979621]

56. Segura MF, et al. Aberrant miR-182 expression promotes melanoma metastasis by repressing FOXO3 and microphthalmia-associated transcription factor. Proc. Natl. Acad. Sci. U. S. A. 2009; 106:1814–9. [PubMed: 19188590]

57. Caizzi L, et al. Genome-wide activity of unliganded estrogen receptor-α in breast cancer cells. Proc. Natl. Acad. Sci. U. S. A. 2014; 111:4892–7. [PubMed: 24639548]

58. Wang Z, et al. Genome-wide mapping of HATs and HDACs reveals distinct functions in active and inactive genes. Cell. 2009; 138:1019–31. [PubMed: 19698979]

59. Boshnjaku V, et al. Epigenetic regulation of sensory neurogenesis in the dorsal root ganglion cell line ND7 by folic acid. Epigenetics. 2011; 6:1207–16. [PubMed: 21931278]

60. Nye MD, et al. The Transcription Factor GLI1 Interacts with SMAD Proteins to Modulate Transforming Growth Factor β-Induced Gene Expression in a p300/CREB-binding Protein-associated Factor (PCAF)-dependent Manner. J. Biol. Chem. 2014; 289:15495–506. [PubMed: 24739390]

61. Wang Z, et al. Combinatorial patterns of histone acetylations and methylations in the human genome. Nat. Genet. 2008; 40:897–903. [PubMed: 18552846]

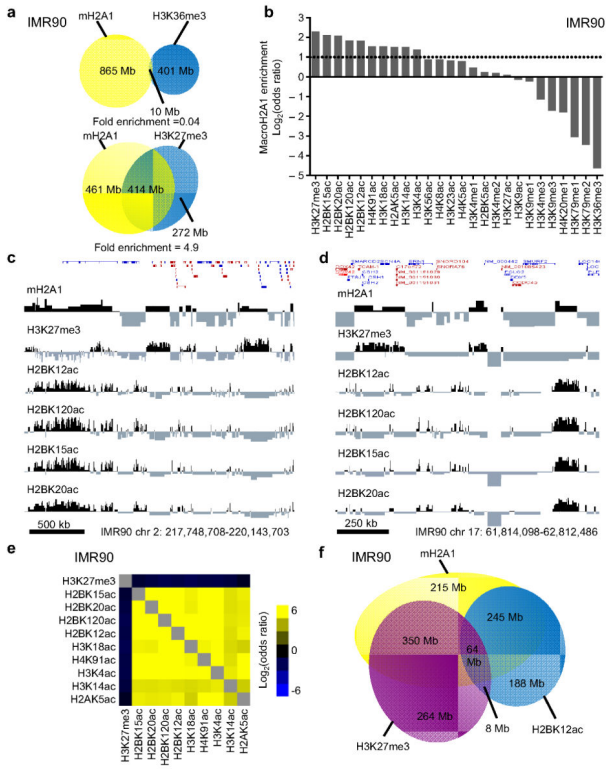

Figure 1.

MacroH2A1 is enriched in two distinct types of chromatin.

(a) Two-way Venn diagrams depicting the overlap between ChIP-seq identified bound regions for macroH2A1 and either H3K36me3 (top) or H3K27me3 (bottom).

(b) ChIP-seq data for macroH2A1 and 26 histone PTMs were analyzed with ISOR to identify regions enriched for each histone mark. The overlap of macroH2A1 with each PTM is expressed as the $\log_2$ of the odds ratio.

(c and d) Genome-browser tracks depicting the relative levels of the indicated histone marks in IMR90 cells. The locations of RefSeq genes are indicated at the top. Blue and Red correspond to plus and minus strand genes, respectively. Scale bars and genomic locations are indicated at bottom.

(e) Hierarchical clustering of an all-to-all comparison of the overlap (expressed as Log_2 odds ratio) of each of the ten histone marks most highly associated with macroH2A1 in IMR90 cells.

(f) Three-way Venn diagram depicting the overlap of macroH2A1 (yellow), H3K27me3 (purple) and H2BK12ac (blue). Numbers indicate the amount of DNA (Mb) in each section.

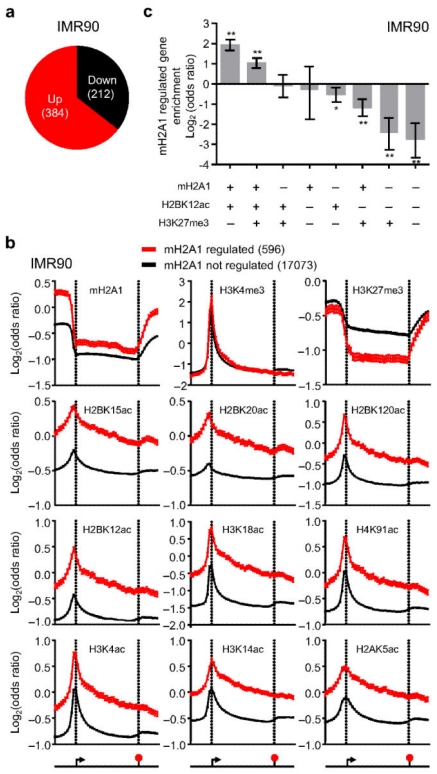

Figure 2.

MacroH2A1-regulated genes are marked by specific histone acetylations.

(a) Pie chart depicting the fraction of genes positively and negatively regulated by macroH2A1 depletion in IMR90 cells using RNA-seq with a cutoff of absolute Log_2 fold change of 0.6 and a $p < 0.05$ (n = 3 independent cell cultures).

(b) Meta-gene analysis of ChIP-seq data for the indicated histone marks from IMR90 cells. Genes were separated into macroH2A1-regulated (n=596) and unregulated groups (n=17,073). The data in each group represent ten 1 kb windows upstream of the TSS, 30 windows spanning the gene body, and ten 1 kb windows downstream of the end of the gene. The vertical dotted lines depict the location of the TSS (left) and the end of the gene (right).

(c) All genes were divided into eight categories based on the presence of macroH2A1, H2BK12ac and H3K27me3 (see Supplementary Fig. 4). The enrichment of macroH2A1-regulated genes in each of the eight classes is expressed as the log_2 odds ratio. Error bars, 95% confidence interval. * $p < 0.01$; ** $p < 1\times10^{-9}$ from Fisher's exact tests.

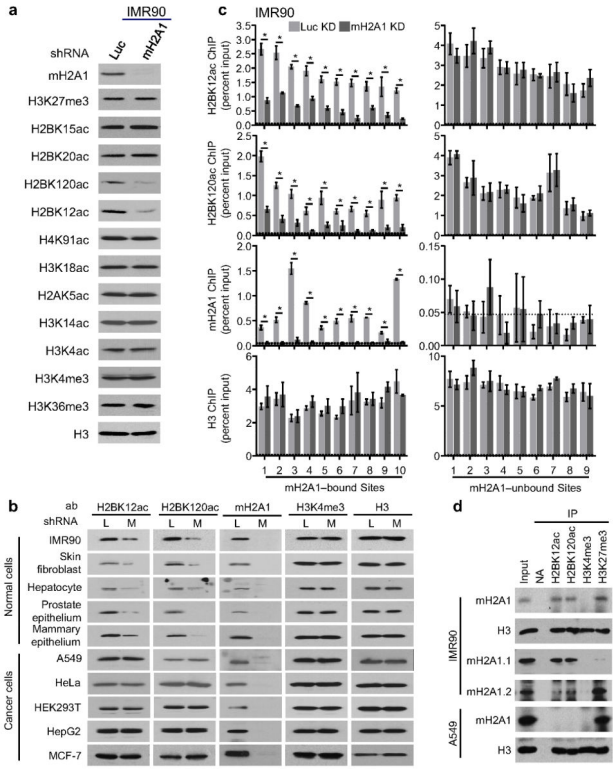

Figure 3.

MacroH2A1 directly regulates the acetylation of H2B at K12 and K120 in primary cell types but not in cancer cells.

(a) Immunoblots for macroH2A1 (mH2A1), histone H3 (H3) and the indicated histone PTMs in IMR90 cells expressing an shRNA against either Luciferase (Luc) as a control or macroH2A1.

(b) Immunoblots for macroH2A1, H3 and the indicated histone marks in primary lung and skin fibroblasts, primary hepatocytes, primary prostate and mammary epithelial cells, A549 lung cancer cells, HeLa cervical carcinoma cells, HEK293T transformed embryonic kidney cells, HepG2 hepatocellular carcinoma cells and MCF-7 breast cancer cells expressing an shRNA against either Luciferase (L, as a control) or macroH2A1 (M).

(c) ChIP-qPCR for H2BK12ac, H2BK120ac, macroH2A1 and histone H3 from IMR90 cells expressing an shRNA directed against either Luciferase (Luc, as a control) or macroH2A1 at H2BK12ac and H2BK120ac positive regions who are either positive (left) or negative (right) for macroH2A1 chromatin incorporation. The horizontal dotted line indicates upper limit of the 95% confidence interval of the signal from no-antibody negative control ChIPs. Error bars, +/− s.e.m. (n = 3 independent cell passages). *$p < 0.05$ from two-tailed Student's t-tests.

(d) Immunoprecipitation with antibodies directed against the indicated PTMs or no antibody (NA) as a control of mononucleosomes from either IMR90 primary lung fibroblasts or A549 lung cancer cells. Immunoblots were performed for both macroH2A1 and histone H3.

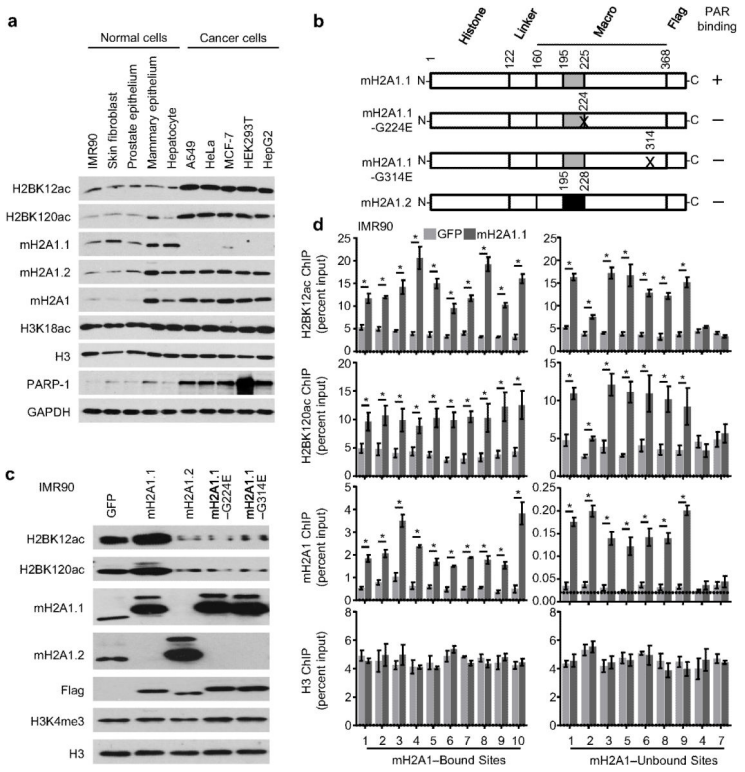

Figure 4.

The macroH2A1.1 is specifically required to regulate H2B K12 and K120 acetylation.

(a) Immunoblots for the indicated factors and histone marks in the normal and cancer cell lines described in Figure 3b.

(b) Schematic depicting the macroH2A1 ectopic expression constructs used in (c). The names and locations of the conserved histone-like region, linker and macrodomain are indicated. Each construct contains a carboxyl-terminal Flag-tag. The location of the glycine to glutamic acid mutations are indicated with an “X”. The regions encoded by the macroH2A1.1 and macroH2A1.2 specific exons are marked in grey and black, respectively. The ability of each protein to bind PAR is indicated with a plus or minus symbol at the right.

(c) Immunoblots for the indicated histone marks from IMR90 cells expressing the macroH2A1 constructs described in (b). Expression of GFP was used as a negative control.

(d) ChIP-qPCR for H2BK12ac, H2BK120ac, macroH2A1 and histone H3 from IMR90 cells expressing macroH2A1.1 or GFP as a control at H2BK12ac and H2BK120ac positive regions who are either positive (left) or negative (right) for macroH2A1 chromatin incorporation. The horizontal dotted line indicates upper limit of the 95% confidence interval of the signal from no-antibody control ChIPs. Error bars, +/− the s.e.m. (n = 3 independent cell passages). *$p < 0.05$ from two-tailed Student’s t-tests.

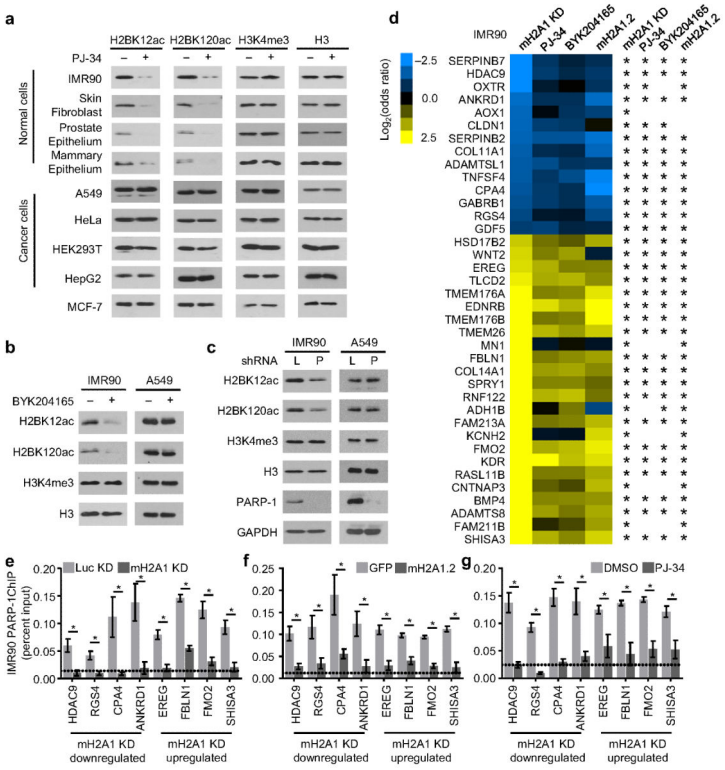

Figure 5.

MacroH2A1.1 and PARP-1 enzymatic activity are required to regulate H2BK12ac and H2BK120ac and macroH2A1-target gene expression.

(a) Immunoblots for macroH2A1, H3 and indicated PTMs from the indicated primary and cancer treated with or without 10 μM of PJ-34 for three days.

(b) Immunoblots for macroH2A1, H3 and indicated PTMs in IMR90 primary lung fibroblasts and A549 lung cancer cells treated with or without 10 μM BYK204165 for three days.

(c) Immunoblots for macroH2A1, H3 and indicated PTMs from IMR90 primary lung fibroblasts and A549 lung cancer cells expressing shRNA against Luciferase (L, as a control) or PARP-1 (P).

(d) (left) Heat map depicting the fold change of macroH2A1-target genes upon macroH2A1 depletion (mH2A1 KD), treatment with 10 μM PJ-34 for two days, treatment with 10 μM BYK204165 for two days, or ectopic expression of macroH2A1.2 (mH2A1.2). (right) * p value < 0.05 from two-tailed Student's t-tests for the indicated gene and condition (n = 3 independent cell passages).

(e) ChIP for PARP-1 at the indicated genes from IMR90 cells expressing shRNA against either Luciferase (L) or macroH2A1 (M). Dotted line indicates upper 95% confidence interval of signal from no-antibody control ChIPs. Error bars, +/− the s.e.m. (n = 3 independent cell passages). *p < 0.05 from two-tailed Student's t-tests.

(f) As for (e) except with IMR90 cells expressing ectopic GFP (as a control) or macroH2A1.2 (mH2A1.2).

(g) As for (e) except with IMR90 cells treated with or without 10 μM PJ-34 for three days.

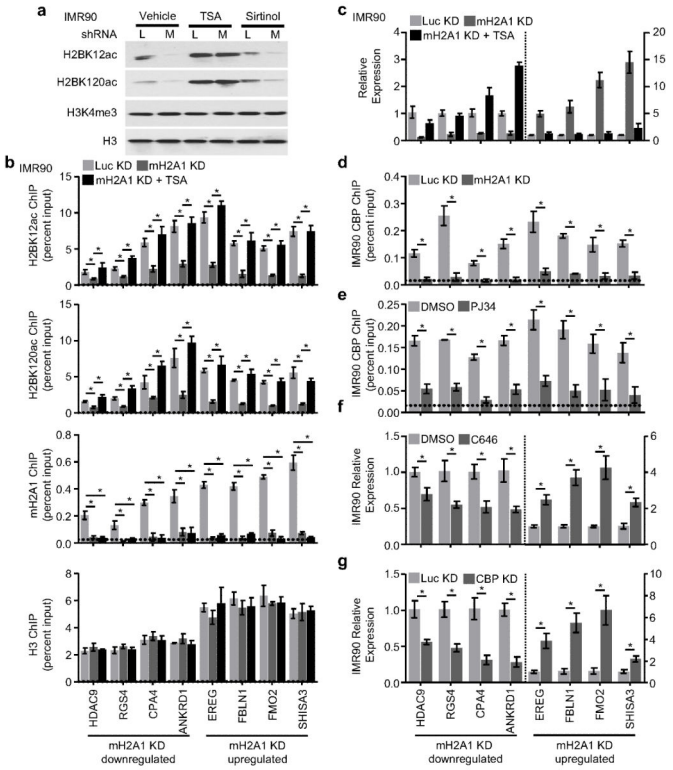

Figure 6.

MacroH2A1 and PARP-1 recruit CBP to mediate acetylation of H2B K12 and K120 and regulate macroH2A1-target gene expression.

(a) Immunoblots for H2BK12ac, H2BK120ac, H3K4me3 or H3 of acid-extracted lysates from IMR90 cells expressing shRNA against luciferase (L) as a control or macroH2A1 (M), either untreated, treated with 25 nM of TSA or 75 μM of Sirtinol for 24hrs.

(b) ChIP for H2BK12ac, H2BK120ac, macroH2A1 and H3 from IMR90 cells expressing shRNA targeted against luciferase (L) as a control or macroH2A1 (M). Cells were treated with 25 nM of TSA where indicated. The horizontal dotted line, upper limit of the 95% confidence interval of the signal from no-antibody control ChIPs. Error bars, +/− s.e.m. (n = 3 independent cell passages). *$p < 0.05$ from two-tailed Student's t-tests.

(c) Reverse transcription coupled to qPCR (RT-qPCR) of IMR90 cells described in (b) for the indicated genes. Downregulated and upregulated genes are plotted on the left or right y-axis, respectively. Error bars, +/− s.e.m. (n = 3 independent cell passages). *$p < 0.05$ from two-tailed Student's t-tests.

(d) ChIP for CBP at indicated genes from IMR90 cells expressing shRNA against either Luciferase (L) or macroH2A1 (M). Horizontal dotted line, upper limit of a 95% confidence interval of signal from no-antibody control ChIPs. Error bars, +/− s.e.m. (n = 3 independent cell passages). *$p < 0.05$ from two-tailed Student's t-tests.

(e) As for (a) except IMR90 cells treated with or without 10 μM PJ-34 for three days.

(f) RT-qPCR for the indicated genes in IMR90 cells treated with or without 20 μM of CBP inhibitor C646 for 3 days. Error bars, +/− s.e.m. (n = 3 independent cell passages). *$p < 0.05$ from two-tailed Student's t-tests. Downregulated and upregulated genes are plotted on the left or right y-axis, respectively.

(g) RT-qPCR as described in (f) except IMR90 cells expressing shRNA against luciferase (L) as a control or CBP.

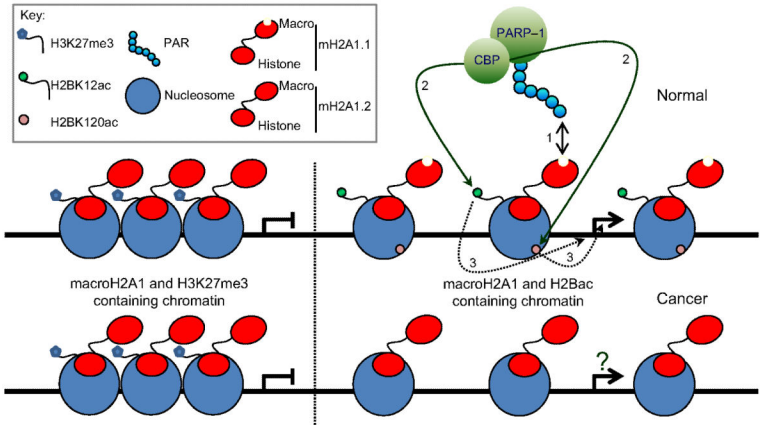

Figure 7.

CBP is recruited to macroH2A1-target genes in a macroH2A1 and PARP-1 dependent fashion.

Model depicting the distinct roles of macroH2A1 in its two chromatin environments. (top) In regions of macroH2A1 and H3K27me3 co-occupancy, loss of macroH2A1 is not sufficient to alter expression of genes, perhaps due to redundant layers of transcriptional repression in these regions. (1) In regions containing both macroH2A1 and H2B acetylations, macroH2A1.1 recruits PARP-1 and CBP to macroH2A1-target genes. (2) CBP promotes H2BK12ac and H2BK120ac. (3) This leads to regulation of genes within these regions. (bottom) The role of macroH2A1 is altered dramatically in cancer. While macroH2A1.2 is present in H3K27me3-containing chromatin, macroH2A1.1 is lost from H2B acetylated regions.

Table 1
Top functional annotations enriched among macroH2A1-regulated genes

Diseases or Functions Annotation	mH2A1 regulated adj. P value[a]	mH2A1 downregulated adj. P value[a]	mH2A1 upregulated adj. P value[a]
Cancer	5.35×10^{-36}	1.79×10^{-10}	5.64×10^{-25}
abdominal neoplasm	3.05×10^{-32}	2.43×10^{-7}	3.78×10^{-25}
female genital neoplasm	8.53×10^{-30}	1.45×10^{-6}	1.32×10^{-23}
genital tumor	9.88×10^{-30}	2.78×10^{-7}	2.10×10^{-22}
uterine tumor	1.10×10^{-27}	5.41×10^{-4}	2.06×10^{-25}
abdominal cancer	1.59×10^{-27}	1.30×10^{-6}	3.76×10^{-21}
endometrial cancer	3.51×10^{-26}	5.32×10^{-3}	1.08×10^{-25}
epithelial neoplasia	5.38×10^{-25}	2.38×10^{-7}	2.27×10^{-17}
genital tract cancer	5.89×10^{-24}	1.58×10^{-5}	8.96×10^{-19}
female genital tract cancer	3.07×10^{-23}	8.14×10^{-5}	4.77×10^{-19}

[a] P values obtained from IPA were corrected for multiple testing with the Benjamini-Hochberg method.